UDK 543.428.3:620.193:67.017
Original scientific article/Izvirni znanstveni članek

ISSN 1580-2949
MTAEC9, 55(4)577(2021)

CORROSION-BEHAVIOR ANALYSIS OF A Fe-Al LAYER IN SEAWATER CHARACTERIZED BY STATIC CHEMICAL ETCHING

STATIČNO KEMIJSKO JEDKANJE KOT ANALIZA KOROZIJSKEGA OBNAŠANJA Fe-Al PREVLEKE V MORSKI VODI

Ningning Li[1,2], Guang Chen[2*], Guoyuan Sun[1], Xinhua Qi[1]

[1]School of Materials Science and Engineering, North China University of Water Resources and Electric Power, Zhengzhou 450045, P.R. China
[2]MIIT Key Laboratory of Advanced Metallic and Intermetallic Materials Technology, Engineering Research Center of Materials Behavior and Design, Ministry of Education, Nanjing University of Science and Technology, Nanjing 210094, P.R. China

Prejem rokopisa – received: 2020-10-12; sprejem za objavo – accepted for publication: 2021-05-27

doi:10.17222/mit.2020.236

The static corrosion behavior of a Fe-Al layer was investigated with an immersion test in seawater, using XRD and SEM with EDS, testing the corrosion rate. The results showed that phases α-Al_2O_3, Fe_2O_3 and MgO were the main corrosion products on the Fe-Al layer surface, while corrosion pits and holes were also observed. It was found that the Fe-Al layer fabricated at 750 °C exhibits a better corrosion resistance, having smaller corrosion pits and holes and also a low corrosion rate. This was related to a good formation ability of the alumina passive film.

Keywords: Fe-Al layer, static corrosion, corrosion pits, corrosion rate

Avtorji so v članku raziskovali korozijsko obnašanje Fe-Al prevleke s preizkusom njenega potapljanja v morski vodi. Preiskave so izvajali s pomočjo rentgenske difrakcije (XRD), vrstične elektronske mikroskopije (SEM) z energijsko disperzijsko spektroskopijo (EDS) in meritvami hitrosti korozije. Rezultati raziskav so pokazali, da so nastali glavni korozijski produkti α-Al_2O_3, Fe_2O_3 in MgO na površini Fe-Al prevleke, opazili pa so tudi pojav korozijskih jamic in luknjic. Avtorji ugotavljajo, da ima Fe-Al prevleka izdelana pri 750 °C boljšo odpornost proti koroziji kot tista izdelana pri 650 °C, ravno zaradi zanemarljive velikosti korozijskih jamic in luknjic. Posledično je tudi hitrost korozije manjša. Razlog za to je tudi dokaj dobra tvorba pasivnega filma aluminijevega oksida.

Ključne besede: Fe-Al prevleka, statična korozija, korozijske jamice, hitrost korozije

1 INTRODUCTION

Fe-Al intermetallic compounds are often used as traditional engineering materials, due to their low density, high-temperature strength, outstanding oxidation and corrosion resistance.[1,2] In recent years, many studies have been made, acquiring great achievements in the application of Fe-Al as a surface protective layer, prepared with various methods. For example, T. Chrostek et al.[3] researched the functional and fractal properties of Fe-Al coatings deposited by gas-detonation spraying. Other scholars studied different methods of preparing a Fe-Al layer, such as hot-dip aluminizing, mechanical alloying, slurry aluminizing and pack aluminizing.[4–7] It is generally known that pack aluminizing is a common method used to obtain a Fe-Al layer, as an in-situ chemical vapor deposition (CVD) process, which has the advantages of a simple operation, stable process and good quality. S. Majumdar et al.[7] discussed pack aluminizing and heat treatment with respect to the phase transition of the Fe-Al layer.

In addition to focusing on the preparation methods, the properties of a Fe-Al layer such as high-temperature oxidation,[8] corrosion[9] and wear resistance were also studied.[10] The aqueous corrosion behavior of a Fe-Al layer at room temperature was studied after detonation gun spraying[11] and double-glow plasma surface alloying.[12] Typically, S. Cezary et al.[11] studied the electrochemical corrosion of a Fe-Al layer in NaCl and H_2SO_4 solutions, prepared by detonation gun spraying, and the results indicate that the layer can be used in aggressive environments. A similar study by X. L. Zhu et al.,[12] who investigated the corrosion properties of a Fe-Al layer in Na_2S and Na_2SO_4 + NaCl solutions, prepared with double-glow plasma surface alloying. The commonly used methods for studying the corrosion behavior are electrochemical and static etching.[11,13,14] The weight-loss technique is often used to determine the corrosion rate in static etching.[14]

The main purpose of this paper is to investigate the static corrosion property of a Fe-Al layer in artificial seawater, prepared with pack aluminizing. The corrosion product phase, morphology and chemical composition were characterized, especially the corrosion rate.

2 EXPERIMENTAL PART

2.1 Materials

The substrate used was low-carbon steel Q235, whose nominal chemical composition is shown in **Ta-**

*Corresponding author's e-mail:
gchen@njust.edu.cn (Guang Chen)

ble 1. Detailed experimental procedures of pack aluminizing used on steel was described in our preliminary work and the main conclusions were already analyzed and discussed.[14] In short, the substrates were aluminized at 650 °C or 750 °C, using a pack-powder mixture composition of 8Al-87Al_2O_3-5$AlCl_3$ (*w*/%). The content of Al in the Fe-Al layer fabricated at 650 °C (73.02 *x*/%) was slightly higher than at 750 °C (72.49 *x*/%). Both layers were composed of the Fe_2Al_5 and $FeAl_3$ phases, but the Fe-Al layer formed at 750 °C contained more Fe_2Al_5.[14]

Table 1: Nominal chemical composition of Q235 low-carbon steel (*w*/%)

Composition	C	Mn	Si	S	P	Fe
Content	0.140–0.220	0.300–0.650	0.300	≤0.050	0.045	Bal.

2.2 Static corrosion test

The solution for the static corrosion test was artificial seawater. Its composition is shown in **Table 2** and it is in line with GB/T 17848-1999 (China).[15] Samples were immersed in artificial seawater at room temperature for 30 days. After (3, 5, 10, 20, 30) days, the samples were taken out of the solution. The standard weight-loss test was carried out in accordance with GB/T 7901-1999 (China).[16] Corrosion products were cleaned with ultrasonic, mechanical or chemical methods. Before and after the tests, the samples were weighed using a digital balance with a precision of 0.0001 g. Each sample was weighted three times to obtain accurate results. During the whole immersion period, the solution was refreshed every seven days.

Table 2: Chemical composition of artificial seawater (g/L)

Component	Content (g/L)	Component	Content (g/L)
NaCl	24.530	$NaHCO_3$	0.200
$MgCl_2{\cdot}6H_2O$	11.110	KBr	0.100
Na_2SO_4	4.090	$SrCl_2{\cdot}6H_2O$	0.042
$CaCl_2$	1.160	NaF	0.003
KCl	0.700	H_3BO_3	0.027

2.3 Surface characterization

The phase identification of corrosion products was carried out using X-ray diffraction (XRD) with CuK_α radiation (D/Max-RA, Rigaku, Japan). Then the morphology and chemical composition were tested using SEM and energy-dispersive spectroscopy (EDS) (S-3400II, Hitachi, Japan). The pit morphology also was observed with SEM. The cross-section morphology and composition after the corrosion also were detected.

3 RESULTS AND DISCUSSION

3.1 Corrosion-product phase

During the immersion, red reactants appeared on the Q235 steel surface after 12 h, but there was no obvious change noticed on the two Fe-Al layer surfaces. However, eight days later, white loose products emerged on the layer surface. **Figure 1** illustrates the XRD patterns for different material surfaces after the corrosion.

The results show that Fe_2O_3 and $CaCO_3$ are the main phases of the steel after the corrosion (**Figure 1a**). Thus, it can be seen that the oxidation of Fe ions mainly occurred on the Q235 steel. The phases of Fe_2Al_5, α-Al_2O_3, Fe_2O_3 and MgO are the main components of the Fe-Al layer, prepared at 650 °C and 750 °C (**Figures 1b** and **1c**). The α-Al_2O_3 and Fe_2O_3 phases are the reaction products, formed when steel is in contact with dissolved oxygen in seawater. Internal aluminium atoms are sufficient for the formation of the alumina passivation film. The $FeAl_3$ phase was not detected, which is confirmed by the results.

3.2 Corrosion-product morphology and chemical composition

After etching, two different regional characteristics were found for two parts of the low-carbon steel surface, namely the anode and cathode area. This is related to the distribution of dissolved oxygen. The potential difference between the cathode and anode of the steel surface is the driving force for the corrosion battery.[17] Metal oxidation occurred on the anode region, forming a low potential area. In contrast, oxygen-reduction reactions arose

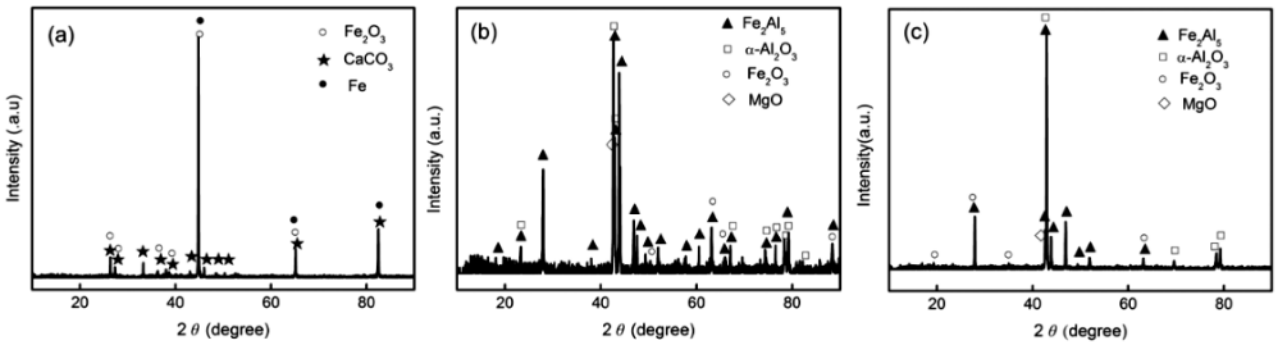

Figure 1: XRD patterns for different material surfaces after corrosion: a) Q235 steel, b) Fe-Al layer fabricated at 650 °C, c) Fe-Al layer fabricated at 750 °C

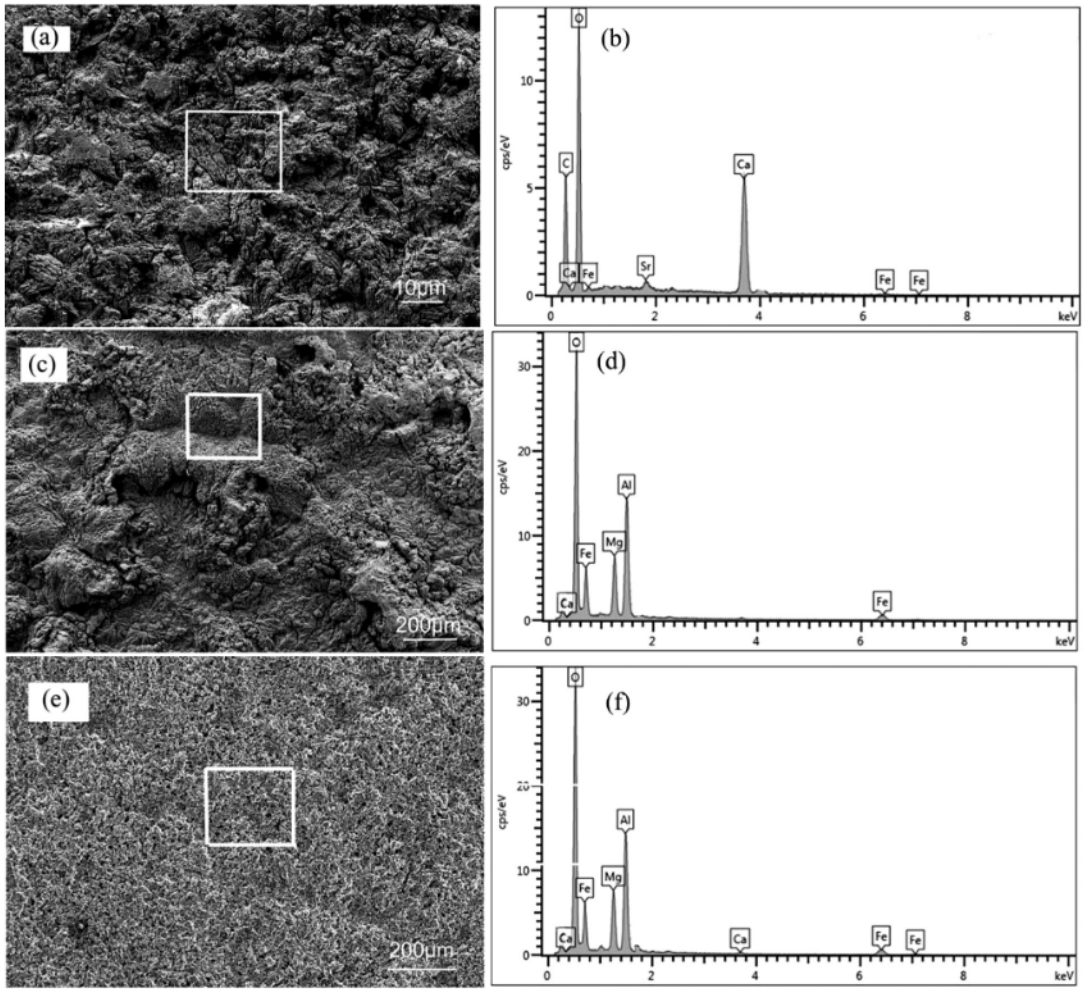

Figure 2: SEM images of corrosion products and EDS spectra of different materials: a) and b) Q235 steel; c) and d) Fe-Al layer fabricated at 650 °C; e) and f) Fe-Al layer fabricated at 750 °C

in the cathode region, forming a high potential area. Finally, corrosion products were accumulated on the cathode, while corrosion holes emerged on the anode. The corrosion morphologies and energy spectra for different materials are shown in **Figure 2**.

Figures 2a and **2b** represent the morphology and energy spectrum of the Q235 steel. It can be seen that the low-carbon steel became uneven. The corrosion products include C, O, Ca, Fe and Sr. This is consistent with the XRD results, but the content of Sr is too low to be detected.

No similar morphology was discovered on the aluminized layer surface, which shows that the dissolved-oxygen distribution has little effect on the corrosion behavior of the aluminized layer. However, corrosion concentrates easily on the edge defects around a sample. The corrosion morphology of the Fe-Al layer fabricated at 650 °C is shown in **Figure 2c**. It can be seen that the products are distributed unevenly on the layer surface, and there is a bubbling phenomenon involving different levels, indicating that the whole corrosion degree is different. The energy spectrum of the Fe-Al layer fabricated at 650 °C is shown in **Figure 2d**. The main elements are O, Mg, Al, Ca and Fe. After binding with oxygen, Fe and Al exist as oxides. This matches with the XRD results mentioned above. The contents of the elements of different materials are shown in **Table 3** below.

Table 3: Element contents after the corrosion of different materials (*w*/%)

Material Elements	Q235	Fe-Al layer fabricated at 650 °C	Fe-Al layer fabricated at 750 °C
C	10.68	–	–
O	50.21	38.98	31.89
Mg	–	7.96	5.02
Al	–	22.07	26.27
Ca	32.13	0.48	0.80
Fe	5.93	30.51	36.02
Sr	1.05	–	–

3.3 Corrosion-pit morphology

As mentioned before, there were corrosion holes on the anode area of the Q235 steel surface, shown in **Fig-**

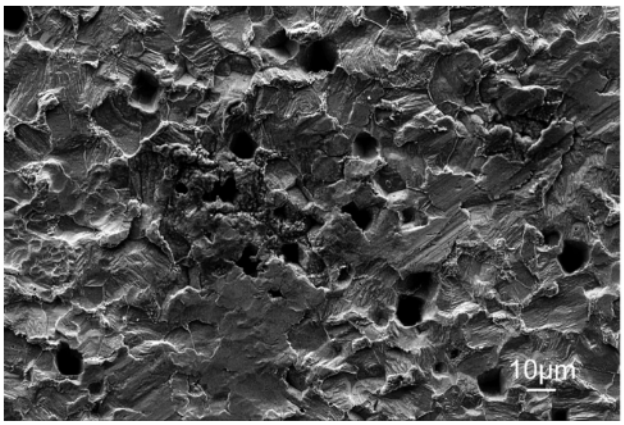

Figure 3: Corrosion-hole morphology of Q235 steel surface

ure 3. The holes are round, approximately 10 μm in diameter and relatively deep. This is related to Cl^- ions that are easy to accumulate on surface defects, such as various grain and phase boundaries, in addition to inclusions.

When the corrosion products were removed, large corrosion pits were found on the surface edge of the Fe-Al layer, fabricated at 650 °C, as shown in **Figures 4a** and **4b**. Moreover, there were round etched holes in other places. The longest radius vector of corrosion pits (about 155 μm) is larger than that of corrosion holes (about 90 μm), and the pit bottom morphology can also

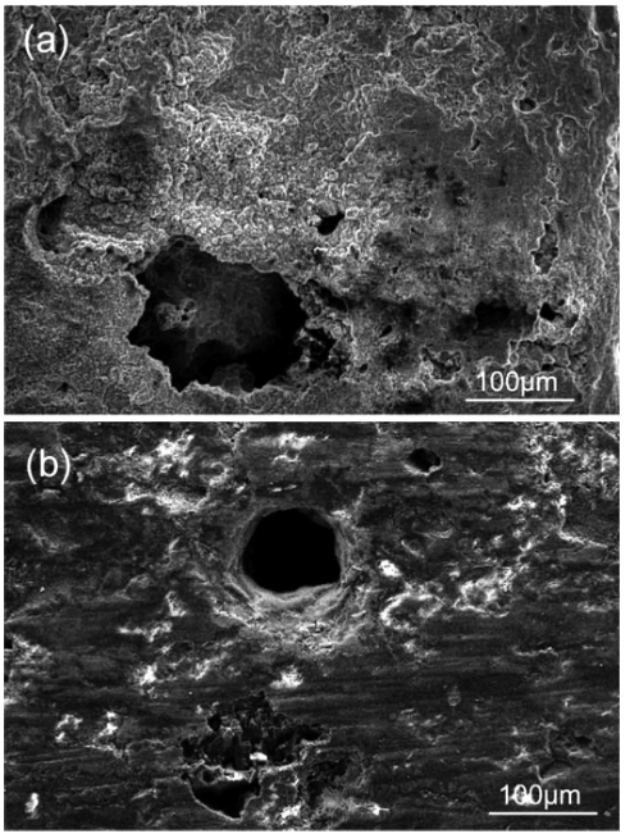

Figure 4: Fe-Al layer surface fabricated at 650 °C: a) corrosion-pit, b) hole morphology

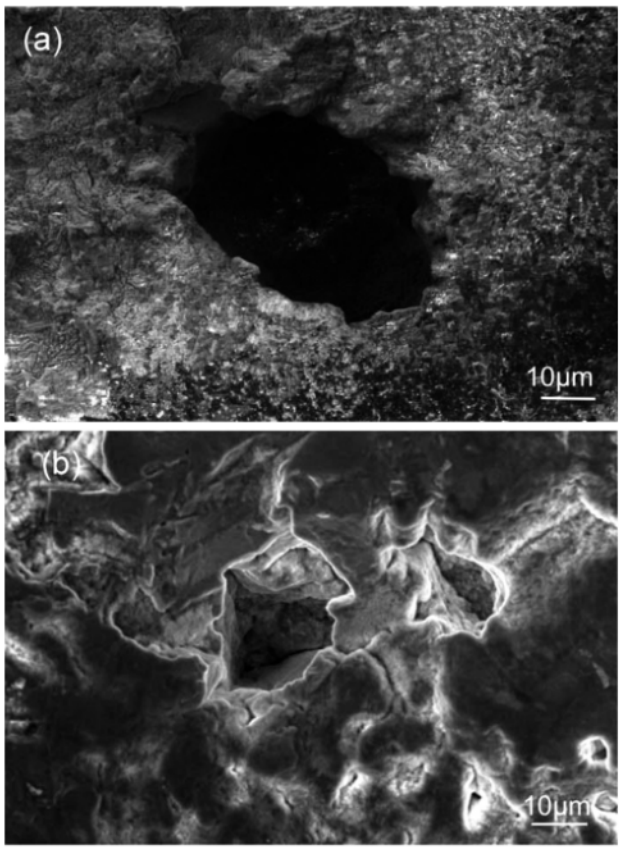

Figure 5: Fe-Al layer surface fabricated at 750 °C: a) corrosion-pit; b) hole morphology

be seen clearly. In addition, the corrosion morphology of the Fe-Al layer formed at 750 °C is shown in **Figures 5a** and **5b**. The corrosion pits and holes also exist on the aluminized layer surface. Here, the pit radius vector (about 56 μm) is larger than that of the hole (about 24 μm), but they are both smaller than that of the Fe-Al layer fabricated at 650 °C. It looks like a triangle from the hole-surface morphology, which is not yet developed into a circle.

Comparing the etching morphologies of the two aluminized layers, it is discovered that the corrosion mainly appears in the original layer defects. Due to the aluminium atoms concentrated at the layer edge and a serious surface roughness, there are many defects. The alumina passive film formed here is relatively weak, therefore easy to be damaged after being in touch with Cl^- ions. This is the cause for corrosion pits. By comparison, the Fe-Al layer fabricated at 750 °C exhibits a better corrosion resistance according to the smaller size captured by the image.

3.4 Cross-section morphology and composition

To study the corrosion products distributed on the Fe-Al layer surface, the cross-section morphology and composition were observed, and they are shown in **Figures 6** to **8. Figures 6a** and **6b** show the corrosion-prod-

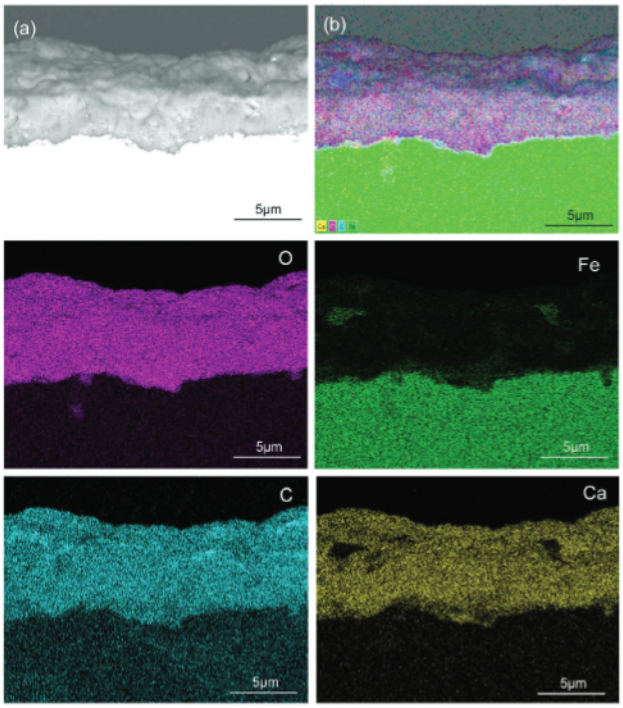

Figure 6: Q235 steel after corrosion: a) cross-section morphology, b) element distribution

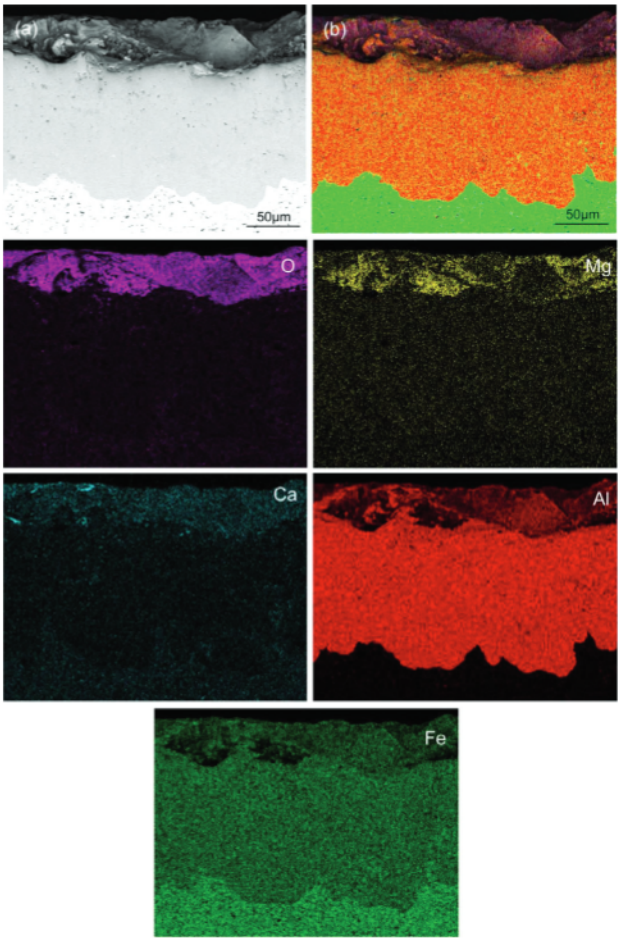

Figure 7: Fe-Al layer fabricated at 650 °C after corrosion: a) cross-section morphology, b) element distribution

uct morphology and general layout of the elements of the Q235 steel after the immersion for 30 days; the other four pictures below show the spread of O, Fe, C and Ca. It can be seen that corrosion products accumulated on the steel surface. Such coverage can hinder the solution diffusion to a certain extent and reduce the etching rate. Results indicated that the corrosion products contain more O, C and Ca, and less Fe. This is in line with the element contents from **Table 3**.

Figure 7 and **8** show the morphology (a) and element distribution (b) of the corrosion products deposited on the Fe-Al layer surface fabricated at 650 °C and 750 °C. Unlike the substrate, the layer surface is covered by a corrosion-product film, mainly consisting of O, Mg, Al, Ca and Fe. The same is also illustrated by the XRD and EDS results, as mentioned above. Both layers proved the existence of the alumina passive film. However, the specific situations of the two Fe-Al layers are also different to some extent. In addition to the Fe_2Al_5 phase, there are still some Al_2O_3 and Fe_2O_3 left, and less MgO. But the phase distributions on the layer surfaces are not the same. There is a large area of the corrosion products covering the Fe-Al layer surface fabricated at 650 °C, and several products are mixed and stacked together. In con-

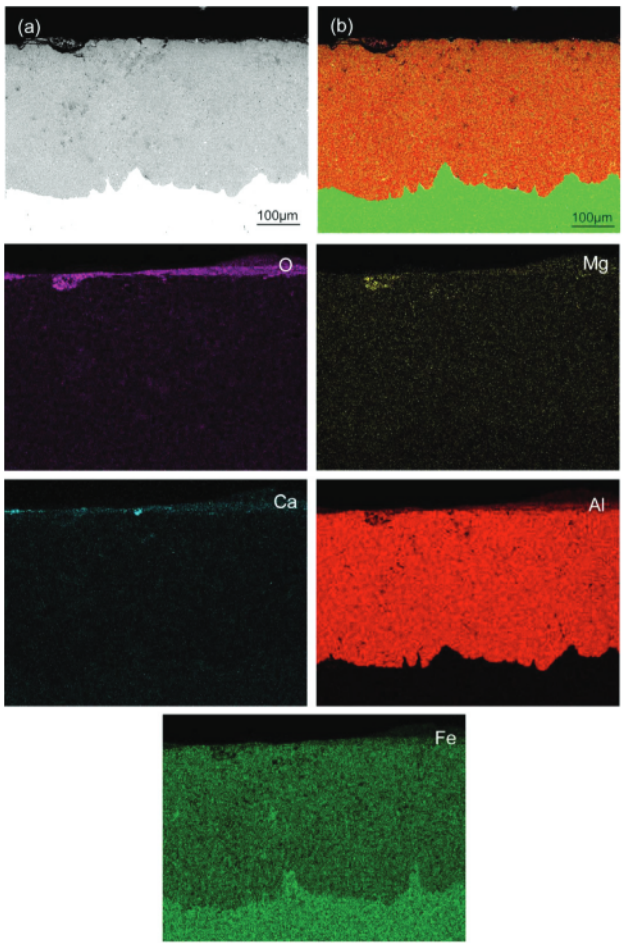

Figure 8: Fe-Al layer fabricated at 750 °C after corrosion: a) cross-section morphology, b) element distribution

trast, the Al_2O_3 passive film covers most of the Fe-Al layer surface, fabricated at 750 °C, while only a small amount of products are accumulated in the corrosion pits. Therefore, the Fe-Al layer fabricated at 750 °C, containing more Fe_2Al_5 phase, exhibits a better performance. This may be due to the strong ability to form a passive film.

3.5 Corrosion rate

According to the above results, the mechanisms of corrosion resistance of different materials were analyzed. For the substrate and two Fe-Al layers, galvanic cells were formed during the etching immersion. Essentially, an electrochemical corrosion reaction occurred, while the current was relatively weak. The oxidation and dissolution of metals in seawater were the main occurrences. First of all, the main chemical reactions of the Q235 low-carbon steel are as follows:

$$Fe + 2OH^- \rightarrow Fe(OH)_2 + 2e^- \quad (1)$$

$$2H_2O + O_2 + 4e^- \rightarrow 4OH^- \quad (2)$$

Fe^{2+} continues to be oxidized to Fe^{3+}:

$$4Fe(OH)_2 + O_2 \rightarrow 4FeOOH + 2H_2O \quad (3)$$

Ca^{2+} ions react with CO_2 which dissolves in seawater to make up $CaCO_3$:

$$Ca^{2+} + H_2O + CO_2 \rightarrow CaCO_3 + 2H^+ \quad (4)$$

As is known to all, the activity of Al is stronger than that of Fe, so the passive film is formed preferentially, followed by the reaction of water with Fe, forming an oxide. The main chemical reactions of the passive-film formation are as follows:

$$Al + H_2O \rightarrow AlOH + H^+ + e^- \quad (5)$$

$$AlOH + H_2O \rightarrow Al(OH)_2 + H^+ + e^- \quad (6)$$

$$Al(OH)_2 \rightarrow AlOOH + H^+ + e^- \quad (7)$$

Total reaction:

$$Al + 2H_2O \rightarrow AlOOH + 3H^+ + 3e^- \quad (8)$$

The typical reactions of a pit formation are as follows:

$$AlOH + Cl^- \rightarrow AlOHCl + e^- \quad (9)$$

$$AlOHCl + Cl^- \rightarrow AlOHCl_2 + e^- \quad (10)$$

After that, attention is paid to the corrosion rate, which is calculated with the weight-loss method. In the light of GB/T 7901-1999 (China),[16] the corrosion depth is commonly used to represent corrosion rate R, with the unit of mm/year. The Equation for the calculation is as follows:

$$R = \frac{8.76\times10^7\times(M - M_1 - M_k)}{STD} \quad (11)$$

The symbols used are as follows: R (mm/year) is the corrosion rate, M (g) is the weight before test, M_1 (g) is the weight after test, M_k is the weight of a blank experiment sample, S (cm^2) is the total surface area of a sample, T (h) is the test time and D (kg/m^3) is the material density.

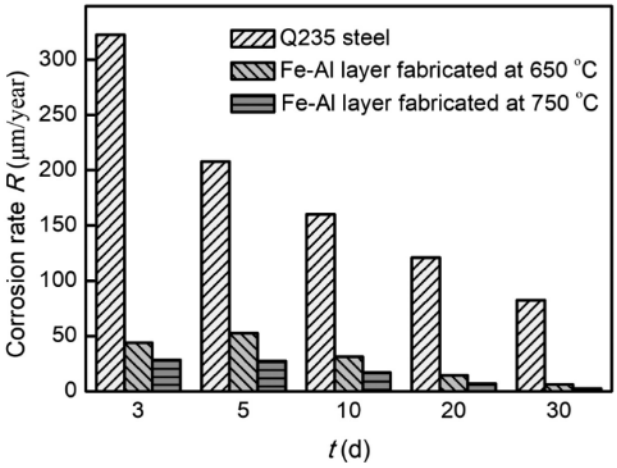

Figure 9: Corrosion rates R of different materials

Figure 9 illustrates the corrosion rates of different materials according to the above formula. It can be clearly seen that the corrosion rate of the Q235 steel is 82.5 μm/year within 30 days, remaining at a high level. In stark contrast, the corrosion rates for the two Fe-Al layers, fabricated at 650 °C and 750 °C, are 6.1 μm/year and 2.3 μm/year, respectively. They are 7.1 % and 2.8 % of the steel corrosion rate, respectively, so the corrosion resistance increased by 92.9 % and 97.2 %. Thus, it can be seen that the Fe-Al layer can reduce the corrosion rate and improve the seawater corrosion resistance.

According to this comparison, the aluminized layer fabricated at 750 °C exhibits a better corrosion resistance. This is related to the surface electrochemical uniformity. The results show that the Al contents in the two Fe-Al layer surfaces are slightly different. For the Fe-Al layer fabricated at 750 °C, the Al content is uniform, including more Fe_2Al_5 phase. As a result, it has a less heterogeneous phase interface and low interface energy, having a good electrochemical uniformity and high-integrity oxide film so that the corrosion reaction kinetic process does not develop easily.

4 CONCLUSIONS

From the study, the following conclusions can be drawn:

(1) Corrosion products on the Q235 steel immersed in seawater are composed of Fe_2O_3 and $CaCO_3$, while α-Al_2O_3, Fe_2O_3 and MgO are the main components of the Fe-Al layer after the immersion.

(2) Corrosion pits and holes are found on the Fe-Al layer surface, owing to the chloride ion contact with the alumina passive film.

(3) The Fe-Al layer fabricated at 750 °C exhibits a better corrosion resistance, having small corrosion pits and holes, and a low corrosion rate.

Acknowledgment

This research was funded by the National Science Foundation of China (Nos. 51571117, 51731006, 51771093 and 91860104) and the High-Level Introduction of Talent Research Start-Up Fund of North China University of Water Resources and Electric Power (No. 4001/40680).

5 REFERENCES

[1] A. Karpuz, H. Kkar, S. Lmeki, M. Ukun, Parametric characterizations of sputtered Fe/Al multilayer thin films, J. Supercond. Nov. Mag., 33 (**2020**) 2, 463–472, doi:10.1007/s10948-019-05207-4

[2] C. J. Cui, C. Q. Ren, Y. Y. Liu, S. Y. Wang, H. J. Su, Directional solidification of Fe-Al-Ta eutectic by electron beam floating zone melting, J. Alloys Compd., 785 (**2019**), 62–71, doi:10.1016/j.jallcom.2019.01.158

[3] T. Chrostek, K. Rychlik, M. Bramowicz, C. Senderowski, Functional and fractal properties of Fe-Al coatings after gas detonation spraying (GDS), Arch. Metall. Mater., 63 (**2018**) 4, 1993–1999, doi:10.24425/amm.2018.125135

[4] W. Zhang, X. J. Guo, H. T. Li, Growth kinetics of Fe-Al alloy layer of hot dip aluminizing with rare earths and computer fitting, Heat Treat. Mat. – UK, 31 (**2006**) 1, 49–52, doi:10.1360/crad20061117

[5] A. Canakci, T. Varol, F. Erdemir, S. Ozkaya, H. Mindivan, Microstructure and properties of Fe–Al intermetallic coatings on the low carbon steel synthesized by mechanical alloying, Int. J. Adv. Manuf. Tech., 73 (**2014**), 849–858, doi:10.1007/s00170-014-5851-2

[6] T. Kepa, F. Pedraza, F. Rouillard, Intermetallic formation of Al-Fe and Al-Ni phases by ultrafast slurry aluminization (flash aluminizing), Surf. Coat. Tech., 397 (**2020**), 126011, doi:10.1016/j.surfcoat.2020.126011

[7] S. Majumdar, B. Paul, V. Kain, G. K. Dey, Formation of Al_2O_3/Fe-Al layers on SS 316 surface by pack aluminizing and heat treatment, Mater. Chem. Phys., 190 (**2017**), 31–37, doi:10.1016/j.matchemphys.2017.01.002

[8] M. Emami, S. M. M Hadavi, S. Hayashi, H. R. Shahverdi, High temperature performance of an FeAl laser coated 9Cr1Mo steel, Oxid. Met., 80 (**2013**), 437–451, doi:10.1007/s11085-013-9415-x

[9] D. R. Yan, Y. Yang, Y. C. Dong, X. Chen, L. Wang, Phase transitions of plasma sprayed Fe-Al intermetallic coating during corrosion in molten zinc at 640 °C, Intermetallics, 22 (**2012**), 160–165, doi:10.1016/j.intermet.2011.10.017

[10] Q. Y. Zhang, Y. Zhou, J. Q. Liu, K. M. Chen, J. G. Mo, X. H. Cui, S. Q. Wang, Wear behavior and mechanism of Fe-Al intermetallic coating prepared by hot-dip aluminizing and diffusion, Metall. Mater. Trans. A, 47 (**2016**), 2232–2242, doi:10.1007/s11661-016-3414-x

[11] C. Senderowski, M. Chodala, Z. Bojar, Corrosion behavior of detonation gun sprayed Fe-Al type intermetallic coating, Materials, 8 (**2015**) 3, 1108–1123, doi:10.3390/ma8031108

[12] X. L. Zhu, Z. J. Yao, X. D. Gu, W. Cong, P. Z. Zhang, Microstructure and corrosion resistance of Fe-Al intermetallic coating on 45 steel synthesized by double glow plasma surface alloying technology, Trans. Nonferr. Metal. Soc., 19 (**2009**) 1, 143–148, doi:10.1016/s1003-6326(08) 60242-3

[13] K. M. Li, X. Y. Shi, F. Xue, J. L. Xie, G. W. Lin, C. N. Pan, Y. Q. Liu, H. Zhang, Static Corrosion Rates of Fused-Cast AZS Refractory Materials by Molten Glass, J. Chin. Ceram. Soc. (Eng), 3 (**2016**) 4, 177–182, doi:10.7521/j.issn.2095-7645.2016.04.04

[14] N. N. Li, M. Z. Wang, Y. S. Li, G. Chen, P. Li, Corrosion behavior of Fe–Al coatings fabricated by pack aluminizing method, Acta Metall. Sin. (Engl. Lett.), 29 (**2016**) 9, 813–819, doi:10.1007/s40195-016-0455-5

[15] Test methods for electrochemical properties of sacrificial anodes, GB/T 17848-1999 (in Chinese)

[16] Metals Materials Uniform Corrosion Methods of Laboratory Immersion Testing, GB/T 7901-1999 (in Chinese)

[17] D. Thirumalaikumarasamy, K. Shanmugam, V. Balasubramanian, Corrosion performance of atmospheric plasma sprayed alumina coatings on AZ31B magnesium alloy under immersion environment, J. Asian. Ceram. Soc., 2 (**2014**) 4, 403–415, doi:10.1016/j.jascer.2014.08.006